Check for updates

Kirigami Structures of Shape Memory Polymer by Femtosecond Laser Scribing and Constrained Heating

Hongshu You, Yachao Zhang, Yanlei Hu,* Yuegan Song, Cheng Xue, Shengyun Ji, Rui Li, Longfu Li, Jiawen Li, Dong Wu,* and Jiaru Chu

Kirigami-inspired structures have found a large variety of applications such as mechanical metamaterials, electronic devices, and biomedicine. In this paper, a facile method is reported to construct deformable Kirigami structures on shape memory polymer with femtosecond laser. Simple slits are scribed using femtosecond laser via an athermal manner and then spontaneously transformed into complicated Kirigami structures under the constrained heating. The deformation process of the Kirigami structures is systematically investigated, which can be accurately predicated by simulation results and thus provide the basis for the programmable structure preparation. The Kirigami structures with controllable deformation are obtained by engineering the initial laser-scribed pattern and heating condition. The method features simplicity, neglectable material loss, and does not need external mechanical force. As a proof of concept demonstration, the as-prepared Kirigami structure is utilized for efficient water harvesting. This work holds great promise in broad applications including mechanical metamaterials and bioinspired functional surfaces.

1. Introduction

Kirigami, the ancient art of paper cutting, has become a new tool for designing reconfigurable and programmable materials.[1] By greatly changing the mechanical properties of materials,[1b,d,2] Kirigami gives materials more flexibility in deformation, and constructs a large number of complex structures.[2a,b,3] UP to now, Kirigami has inspired researchers to engineer various materials (e.g., graphene,[4] gold nanofilm,[5] polymer films)[1c,6] to achieve extensive applications spanning self-assembly of 3D mesostructures,[7] auxetic metamaterials,[3b,8] optical tracking solar cells,[9] and stretchable batteries.[10]

There are two typical schemes for constructing desired Kirigami structures in the view of the way to treat the materials.[3d,4,9,11] One is to directly remove part of the material

in order to obtain hollow structures,[3c,12] which undoubtedly increases the processing complexity and causes material waste. In contrast to the subtractive material processing manner, the other scheme is to introduce slits into the material to construct the required Kirigami structures by subsequent deformation,[1c,3d,4,9,11,13] during which persistent external forces are required to stretching the slits. Then one question arises. Can one realize desired Kirigami structures without materials subtraction and engagement of external force?

Here, we propose a facile fabrication approach to prepare Kirigami microstructures on a shape memory polymer (SMP) film. Simple slits are introduced on a flat shrinkable polystyrene film through an athermal scribing process with femtosecond laser. And then the SMP film is heated under the constrained condition to achieve the desirable programmed shapes. The morphological evolution of various designs such as "L-shaped" slit, right-handed four "L-shaped" slits, parallel slits, and concentric arcs as the heating time is systematically characterized. The transformed shape can be well predicted by numerical simulation, and demonstrated by the experimental results. Inspired by the water harvesting capability of the spider silk, the as-prepared spidery Kirigami structures can be used for efficient water harvesting. Our work broadens the fabrication strategies for engineered Kirigami structure and provides insights for the applications in mechanical metamaterials, flexible electronics, and bioscaffolds.

2. Result and Discussion

2.1. Manufacture Method of the Kirigami Structure Using Femtosecond Laser Scribing and Constrained Heating

The heat shrinkable film used here is a biaxial prestretched SMP film. When the film is heated above the glass transition temperature (T_g), it shrinks to its initial shape. Here, a femtosecond laser (wavelength 1030 nm, repetition rate 100 KHz, pulse duration <400 fs) is employed to scribe across the SMP surface to generate through slits. Note the femtosecond laser processing has ultralow thermal effect, the laser scribing can be considered to be an athermal process which cannot induce any change of the

H. You, Dr. Y. Zhang, Prof. Y. Hu, Y. Song, C. Xue, Dr. S. Ji, R. Li, Dr. L. Li, Prof. J. Li, Prof. D. Wu, Prof. J. Chu
CAS Key Laboratory of Mechanical Behavior and Design of Materials
Key Laboratory of Precision Scientific Instrumentation of Anhui Higher Education Institutes
Department of Precision Machinery and Precision Instrumentation
University of Science and Technology of China
Hefei, Anhui 230 027, China
E-mail: huyl@ustc.edu.cn; dongwu@ustc.edu.cn

**ADVANCED
SCIENCE NEWS**
www.advancedsciencenews.com

**ADVANCED
MATERIALS
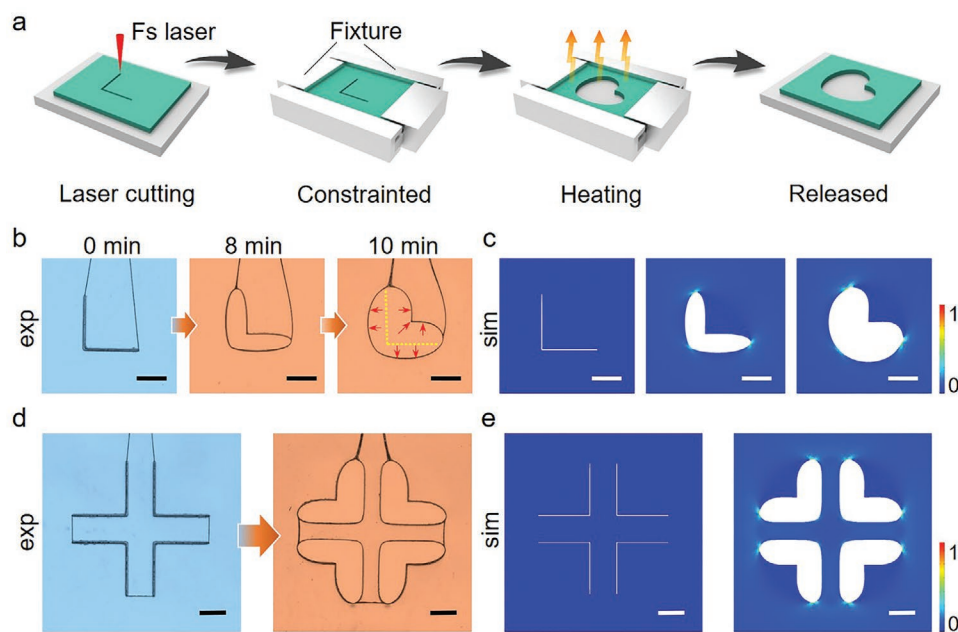TECHNOLOGIES**
www.advmattechnol.de

Figure 1. The shape transformation of the slits scribed by femtosecond laser on the SMP film under constrained condition. a) Schematic process of femtosecond laser scribing and constrained heating. b) The shape transformation of a single "L-shaped" slit with the heating time. c) Simulation results corresponding to (b). d) The shape transformation of four "L-shaped" slits arranged in a centrosymmetric way. e) Simulation results corresponding to (c). Scale bars: 1 mm. For clarity, the images of initial slits are rendered with light blue pseudocolor, and the images of the transformed shape after heating are rendered with orange (The heating time is 10 min, the same hereinafter unless specifically indicated).

SMP. After processing optimization, the minimum width of the slit obtained by femtosecond laser can reach 53 µm. If the SMP is heated above the T_g, the slits shrink with the film and remain closed after heating (Figure S1, Supporting Information). In comparison, by applying constraints around the shrinkable SMP film, the slits expand after heating with the material shrinkage and the four edges of the film are immobile (**Figure 1**a). As the temperature decreases to room temperature, the constraint is released and the shape of the transformed film is fixed. For example, the initial "L-shaped" slit with equal length for both sides is scribed by the femtosecond laser on the film. After heating, the outside edges of the right angle expand and transform into the arc shape. For the inside edges of the right angle, the turning point gradually shifts from the initial site along the diagonal direction and maintains the shape of right angle. Finally, the "L-shaped" slit is transformed into the heart shape after heating for 10 min as shown in Figure 1b. The simulation results shown in Figure 1c are consistent with the experimental results. When four "L-shaped" slits are arranged in a centrosymmetric way (Figure 1d), the transformation is mutually influenced and the outside edges of the right angle keep straight. The turning points get away from the initial site as the same as the single "L-shaped" slit but with a decreased degree. The simulation result is well consistent with the experiment (Figure 1e).

2.2. Preparation and Deformation Process of the Chiral Kirigami Structure

Moreover, when four "L-shaped" slits are arranged in a chiral manner, the right-handed structure undergoes a spontaneous

anticlockwise rotation deformation when heated (**Figure 2**a). In contrast, the clockwise rotation deformation can be obtained by heating the left-handed four "L-shaped" slits. On this basis, the array of structures with opposite rotation direction can be obtained on a single sheet (Figure 2b). It should be noted that the black lines on the sample surface except for the slits are caused by a small amount of pulses hitting the sample when the laser moves between slits. This rotation results from the asymmetric off-center contraction of the four cantilevers. In order to study the deformation dynamics of the chiral slits, simulation analysis is carried out and the results are in consistent with the experiment, as shown in Figure 2c. The evolution of the rotation deformation of the right-handed structure with the heating time is shown in Figure 2d. Crossed lines are distinctly marked in the central region of the structure by laser to help quantifying the rotation of the structure. One can see that the four "L-shaped" beams gradually shrink and turn straight with the heating time, leading to that the central region shrinks and rotates anticlockwise simultaneously. The width of the beam is 572.5 µm before heating and shrinks into 297.2 µm after heating for 15 min. It can also be seen that the crossed light black lines in the central region turn deep black owing to the shrinkage.

To quantitatively investigate the morphological changes of the structure, the rotation angle of the cross-marked center-line (θ) is measured to describe the rotation of the chiral unit (Figure 2e, the initial value is 0°). The duty cycle is measured to describe the shrinkage degree of material (Figure 2f, the initial value is 2.3%). The duty cycle is defined as

$$\eta = S_{blank}/d^2 \tag{1}$$

**ADVANCED
SCIENCE NEWS**
www.advancedsciencenews.com

**ADVANCED
MATERIALS
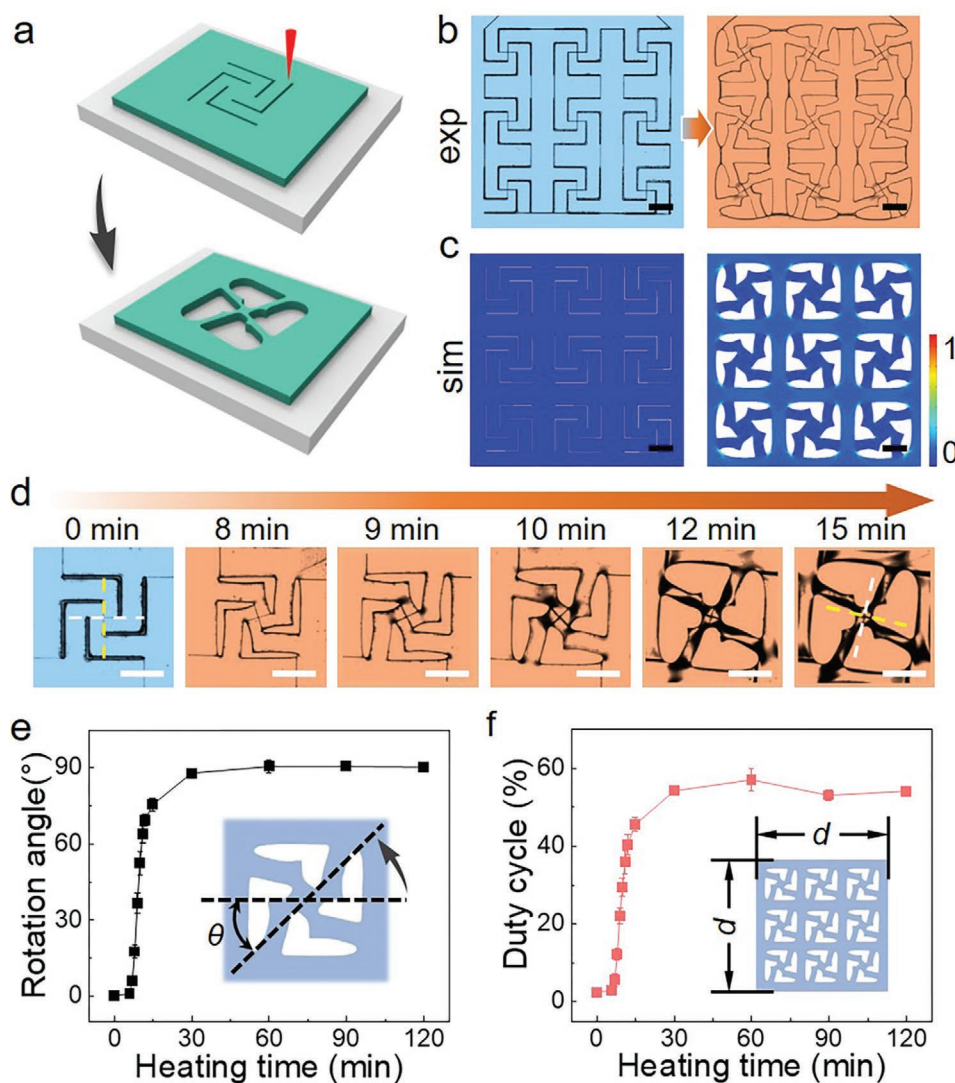TECHNOLOGIES**
www.advmattechnol.de

Figure 2. Self-rotation during shape transformation of chiral Kirigami unit. a) Schematic of laser scribing chiral unit and the self-rotation deformation after heating. b) Array of the chiral Kirigami units with opposite chirality before and after heating. c) Simulation results corresponding to (b). d) The evolution of the rotation deformation of right-handed four "L-shaped" slits with the heating time. e) The quantitative relationship between the rotation angle θ and the heating time. f) The quantitative relationship between the duty cycle and the heating time. Five repeated experiments are performed to obtain the data in (e) and (f). Scale bars: 1 mm.

where S_{blank} is the area of the blank opening formed by the expansion of the slits, d is the side length of the whole region when the fixed constraint is applied. Since the initial temperature of the film is lower than the T_g, the structure has to wait ≈6 min for the temperature rise to start deforming. As long as the temperature reaches the T_g, the structure shrinks and central region rotates accordingly. After heating for 30 min, the θ reaches to ≈90° and keeps stable because of the fully shrinkage of the material (Figure 2e). Similarly, the duty cycle remains unchanged during the beginning 6 min. When the film is heated for 30 min, the duty cycle increases to 54.1% and then stabilizes (Figure 2f). Assuming that this Kirigami pattern is achieved by direct cutting in a subtractive manner, 54.1% of the material is removed and wasted. In contrast, our manufacturing method only causes a waste of 2.3% of the material. More complex chiral Kirigami patterns can be obtained by self-rotation

deformations of simple slits (Figure S2 and Movies S1 and S2, Supporting Information).

2.3. The Programmable Kirigami Patterns Transformed from Parallel Slits

Figure 3a displays two distinct kinds of Kirigami works of fishing net. The grid size of the upper pattern keeps constant, while the pattern in the lower one gradually decreases from one side to the other. We take the grid pattern as an example to investigate the influence of the arrangement of the multiple parallel slits on the whole deformation of the structure. For one straight slit, an elliptical opening is obtained upon full shrinkage (Figure S3, Supporting Information). Figure 3b shows the effect of the relative length of adjacent slits on the
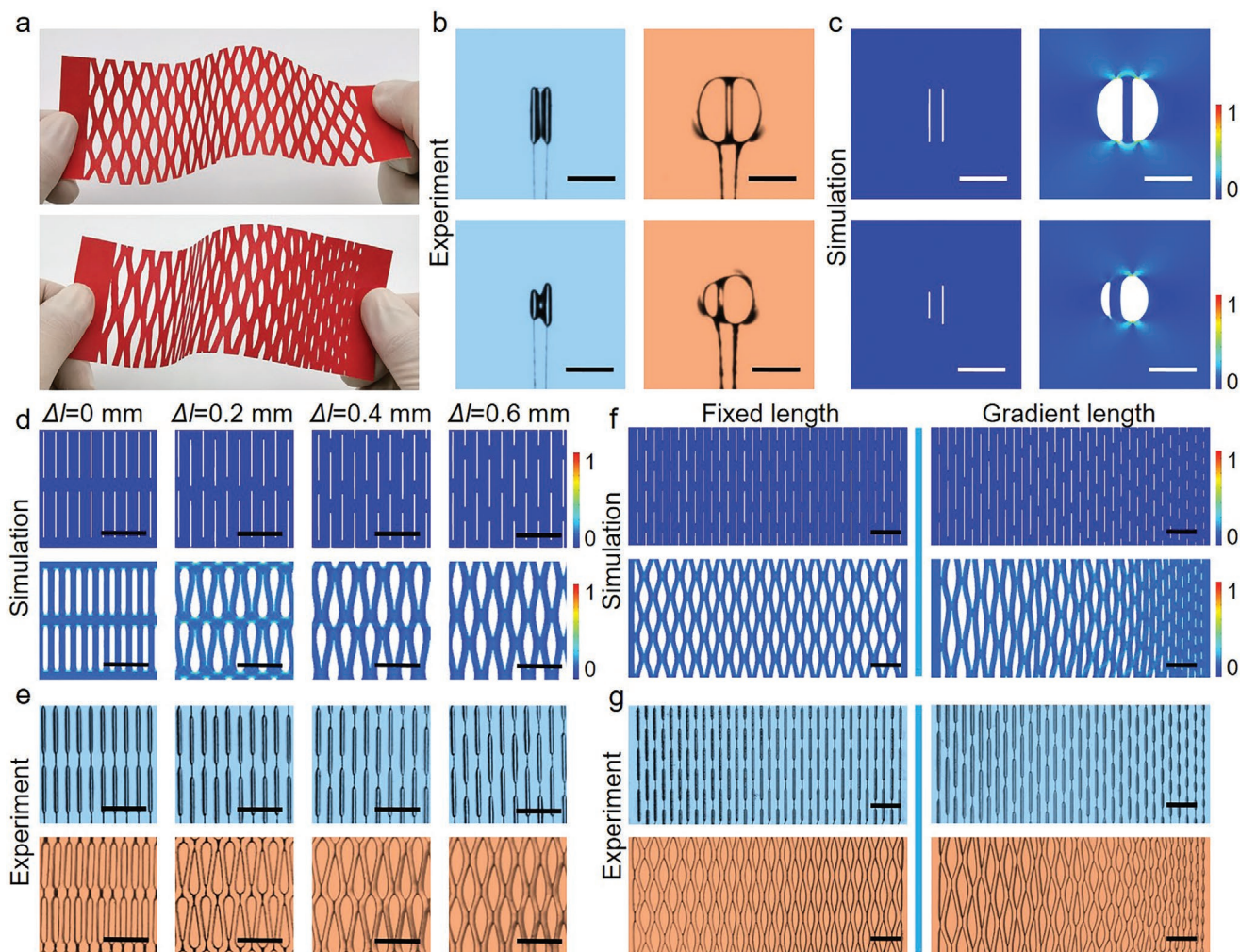
**ADVANCED
SCIENCE NEWS**
www.advancedsciencenews.com

**ADVANCED
MATERIALS
TECHNOLOGIES**
www.advmattechnol.de

Figure 3. The Kirigami patterns transformed from parallel slits with different motifs. a) Kirigami pattern on a paper with uniform grids (upper) and gradient grids (lower). b,c) Shape transformations and the corresponding simulation results of two parallel slits with identical and different lengths, respectively. d,e) Simulation and experimental results of the shape transformations with the parallel slits arranged with increasing position offset in the longitudinal direction, respectively. f,g) Simulation and experimental results of the shape transformations with the parallel slits arranged without (left) and with (right) gradient of slit lengths along the transverse direction, respectively. Scale bars: 1 mm.

deformation. After heating, the two parallel slits with identical length expand to form two symmetrically distributed kidney-bean-like openings. Due to the symmetrical expansion of two slits, the bridge area between the two slits shrinks and form a straight thin rib. After heating, the width of the bridge is reduced from 221.7 to 155.2 μm. In the case of two slits with different lengths, the expansion of the longer slit is much larger than that of the shorter one, giving rise to the shift of the rib to the shorter slit side. As shown in Figure 3c, the simulation results of the above two cases are in good agreement with the experimental ones.

Various shape transformations of the parallel slits array with identical length can be obtained by varying the longitudinal offset of adjacent slits Δl which are predicted by simulation (Figure 3d), the schematic of the design parameters is shown in Figure S4, Supporting Information. For the motif where all the parallel slits are arranged with $\Delta l = 0$ mm, a uniform pattern with long and narrow openings can be obtained. The

deformation of each slit along the longitudinal direction is almost the same. However, for the motif where the parallel slits are arranged with relative position offset in the longitudinal direction ($\Delta l \neq 0$), the expansion of the each slit along the longitudinal direction can be completely different. The part of the slit that does not overlap with adjacent slit in the transverse direction has larger expansion while the overlapped part constrains each other, resulting in a reduced expansion. As a result, the slits arranged with $\Delta l = 0.2$ and 0.4 mm turn into the pattern of water-drop shape, while the slits arranged with $\Delta l = 0.6$ mm (the center of the part between the two slits is close to the center of adjacent slit, Figure S4, Supporting Information) form the spindle shape. According to our measurement, there is no significant difference between the rib width with varying Δl (the rib width is 160.1 μm for $\Delta l = 0$ mm, and 155.3 μm for $\Delta l = 0.6$ mm, respectively). The corresponding experimental results are consistent with the simulation results as shown in Figure 3e. The shape transformations of $\Delta l = 0.1$,

**ADVANCED
SCIENCE NEWS**
www.advancedsciencenews.com

**ADVANCED
MATERIALS
TECHNOLOGIES**
www.advmattechnol.de

0.3, and 0.5 are shown in Figure S5 (Supporting Information). In brief, various uniform Kirigami can be obtained by regulating the position offset of the slits.

Base on the shape transformation results of the parallel slits and simulation (Figure 3f), the desirable fishing net pattern without or with gradient grid size are both obtained by simply laser scribing parallel slits with staggered arrangements (Figure 3g). The slits in the left pattern in Figure 3f have identical length while in the right pattern have length gradient along the transverse direction. Each slit has an identical length in the longitudinal direction. It can be seen that the Kirigami with gradient grids can be conveniently realized using the femtosecond laser scribing and constraint heating. Compared with the direct perforation to obtain the fishing net pattern, our slit-transformation method can significantly save time with the level of 50.04% and 50.21% for uniform pattern and gradient pattern, respectively. In addition, our method can reduce the material waste by 31.36% and 18.77% for uniform pattern and gradient pattern, respectively.

2.4. The Programmable Kirigami Generated by Shape Transformation of Concentric Arc Slits

In addition to the simple straight slits, the shape transformations of arc slits are investigated. Three motifs composed of concentric arc slits with different designs as well as their transformed shape are shown in **Figure 4**a (the schematic of the design parameters is shown in Figure S7, Supporting Information). The arc slits are evenly distributed on each circle, and the

radius of each circle is increased from 250 µm to 3 mm with a constant interval of 250 µm. The slit position here represents the number of turns of the slits. The designed arc length of motif 1 increases from the center to the outside according to the linear relationship as indicated with the black curve in Figure 4b. For motif 2, the designed arc length is identical on each circle. For motif 3, the designed arc length decreases from the center to the outside as the linear relationship as indicated with the blue curve in Figure 4b. Compared with motif 1, the first inner circle is missing in motif 2, while the two inner circles are missing in motif 3 respectively, due to the conflict between the slit length and the size of the central area. The pattern of motif 1 changes greatly with the increased heating time, especially for the heating time exceeding 7 min, as shown in Figure S8 (Supporting Information). During heating, the expansion of the slits in the periphery region is easier than that in the central, and the peripheral slits take up most of the room by further expanding. Eventually, only the outermost four circles of slits gradually open and the inner slits remain closed. As shown in Figure 4c, the width of the opening of a specific circle is obtained by averaging the width of all opening located on the circle. As discussed above, the longer the slit is, the larger the opening is. Moreover, the peripheral slits are easier to expand compared with the center. Therefore, for the motif 1, the slits located within the eight circles remain closed, and the opening width increases sharply for the outer circles. The opening width located at the eleventh circle is 1.087 mm, which is the maximum among the three motifs. For the motif 2, although all the slits have the identical length, the expansion of the outer slits suppress the expansion of the inner ones, thus
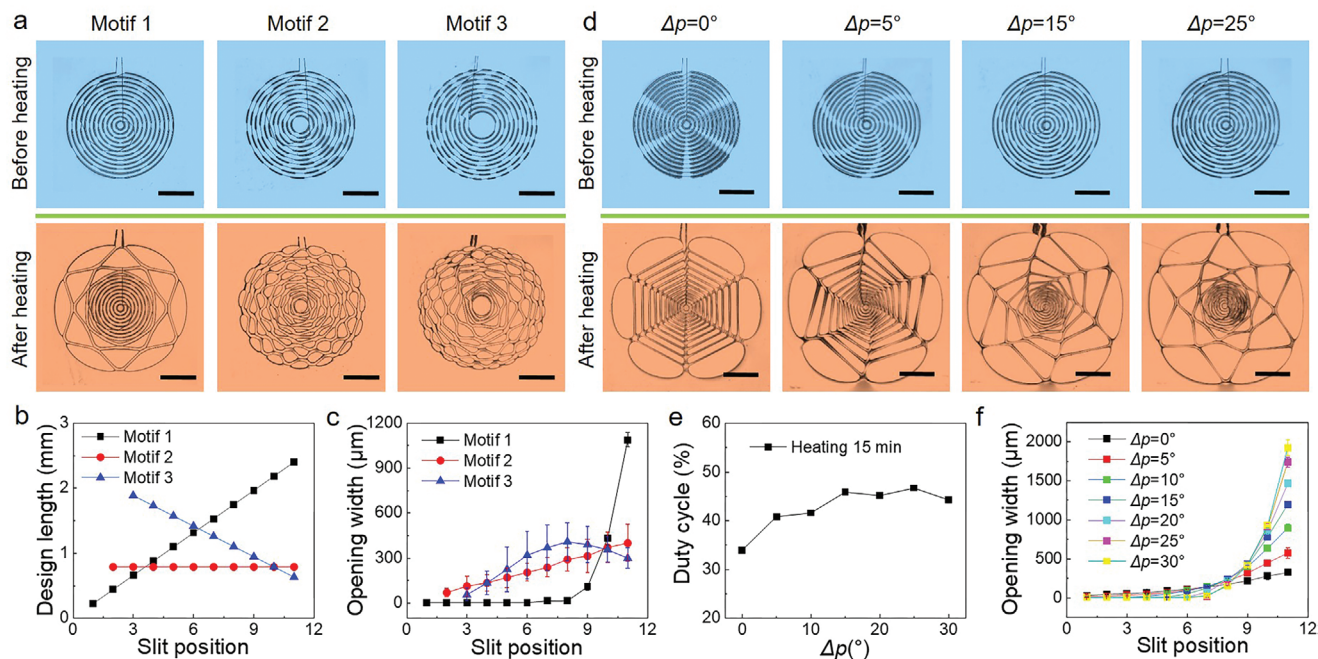

Figure 4. The Kirigami generated by shape transformation of concentric arc slits with different motifs. a) The shape transformation of concentric arcs with different distribution of slits length. b) The relationship between the design length of slit and the position of circle where the slit located for the three motifs in Figure 4a. c) The relationship between the opening width and the slit position for the three motifs in Figure 4a. d) Various spidery Kirigami patterns obtained by regulating Δp (the samples were heated for 15 min). e) The duty cycle of spidery patterns varies with Δp. f) The relationship between the opening width and the slit position for the spidery pattern regulated by Δp. Scale bars: 2 mm.

**ADVANCED
SCIENCE NEWS**

www.advancedsciencenews.com

**ADVANCED
MATERIALS
TECHNOLOGIES**

www.advmattechnol.de

the inner slits expand less and the opening width has a linear dependence on the slit position. For the motif 3, the slit length decreases from the center to the outer, however, due to the suppress effect of the slit in the outer circle, the maximum opening appears at the eighth circle.

In addition to adjusting the length of the arc slits, the spatial arrangement of the slits can also have a significant influence on the shape transformation. The spidery Kirigami patterns are obtained in Figure 4d and Figure S10 (Supporting Information), where Δp denotes the offset angle of the slit relative to adjacent slit on other circles along the anticlockwise direction (the definition of Δp and other parameters of spidery patterns are shown in Figure S9, Supporting Information). The motif 1 in Figure 4a is the pattern when Δp is 30°. When Δp is larger than 30°, for example, Δp = 40°, the deformed pattern can be obtained by simply mirroring the deformed pattern when Δp = 20°. In other words, the Kirigami patterns here are plane rotationally symmetrical patterns with a rotation angle of 60°, so the patterns corresponding to Δp and (60° − Δp) are mirror symmetrical. Similar to the deformation of the parallel slits, greater mutual influence occurs in expansion behavior when the adjacent arcs have more overlapping parts. The duty cycle of the deformed pattern is adopted to describe the degree of

the silts expansion (Figure 4e). After heating for 15 min, the duty cycle varies slightly from 33.9 to 46.7. Figure 4f shows the variation of the slit opening width with the slit location after heating for 15 min. Generally, the expansion of the slits in the periphery region is easier than that in the central as discussed above, and the opening width of the outer circles is much larger than that of inner ones. For the structure of Δp = 0°, all the slits can expand and their width increases slowly with the position. When Δp increases, the difference between the opening width of the outer ring slit and that of the inner ring slit increases, resulting in the steeper curves.

2.5. Water Harvesting Functionality of Spidery Kirigami Pattern

Inspired by the water harvesting function of the spider web (**Figure 5**a), the spidery Kirigami patterns regulated by Δp are used to perform the water harvesting experiment. As shown in Figure 5b, a water droplet of 2 µL is dropped on the surface of the sample to measure the wettability. The contact angle (CA) for pristine and structured SMP film is almost the same (88.2°–88.7°). When subjected to oxygen plasma treatment, the pristine surface becomes hydrophilic and the water CA
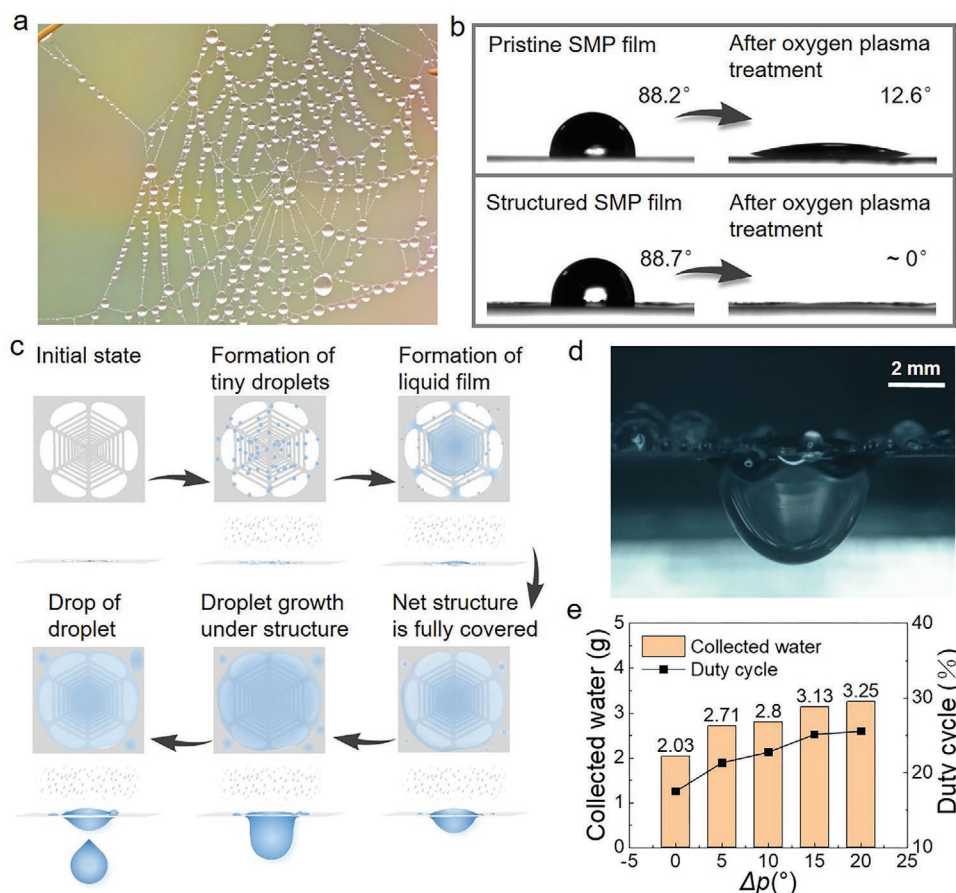

Figure 5. Water harvesting functionality of spidery Kirigami pattern. a) Water droplets are harvested from the air and condensed on the natural spider web. b) The wetting properties of the pristine SMP film, structured SMP film, oxygen plasma-treated SMP film and oxygen plasma-treated structured SMP film. c) Schematic of water collection via the spidery structure. d) Image of water droplets collected by the spidery Kirigami structure. e) The comparison of the collected water mass after 1 h for spidery Kirigami structures with different Δp.

decreases to 12.5°. The spidery Kirigami structure is superhydrophilic with a CA near 0°. The water harvesting experiments are performed on the superhydrophilic spidery structures as shown in Figure 5c. First, the mist in the air condenses on the surface of the structure to form tiny water droplets. Then the droplets become larger and coalesce into a liquid film. After a while, the liquid film penetrates the spidery structure and expands further until the whole structure is covered. As more and more water condenses in the structure, the droplet finally falls off the film under gravity. The remaining water droplet proceeds to grow in volume until it drops. The water droplet on the structure harvested from the mist of the structure is shown in Figure 5d. The condensation process of water droplets is shown in supplementary material movie S3 (Supporting Information). After 1 h, the mass of the collected water with the spidery structures having different Δp is measured and compared as shown in Figure 5e. The mass of the collected water increases with the Δp from 0° to 20° and reaches a maximum of 3.25 g, which is consistent with the tendency of the structures' duty cycle. It indicates that the water mist collection capacity of the Kirigami is determined by the duty cycle of the structures.

3. Conclusion

A facile and nonsubtractive fabrication method is proposed to prepare Kirigami structures based on shape memory polymers. The complicated Kirigami patterns are transformed from simple slits which are scribed on SMP film by femtosecond laser. The deformation dynamics of the SMP structures are systematically investigated by experiments and simulations. The simulation results are consistent with the experimental ones. The dependence of the Kirigami morphology on the laser scribing path and heating time is quantitatively studied. By regulating the geometric parameters and relative position of the slits, one can control the width and shape of the slit opening, and change the duty cycle of the Kirigami structure. The method holds the advantage of neglectable material loss and free of external force. Finally, the application of the spidery Kirigami in water mist harvesting is demonstrated and the influence of the structural parameters on the functionality is revealed. This work unfolds the possibilities for the preparation of transformable mechanical metasurfaces and diverse functional structured surfaces.

4. Experimental Section

Fabrication and Heating: The glass transition temperature of SMP film was about 107 °C. The SMP film of 0.15 mm thickness completely shrank when heated above 115 °C without any constraints, reaching a maximum shrinkage ratio of 60%. AutoCAD 2019 was utilized to design the pattern of slits in the film. Then the CAD file was imported to the computer to guide the laser scanning. The Bluecut femtosecond fiber laser (Menlo systems) with central wavelength of 1030 nm, repetition rate of 100 KHz, pulse duration of <400 fs was used for fabrication. Then, the periphery of the SMP film with slits was fixed by iron clamps. Finally, the sample was placed in an oven and heated at 115 °C. The heating process can be also performed using a hot air gun as demonstrated in movies S1 and S2 (Supporting Information).

Water Harvesting Experiment: The spidery-like Kirigami structure is exposed to oxygen plasma to turn the surface into a superhydrophilic state. The water contact angle of the water droplet ($\approx 2 \mu L$) in air was measured by CA100C (Shanghai Innuo Precision Instruments Co., Ltd., Shanghai, China) via the sessile drop method. The sample was placed in a humidifier environment, and a plastic cup was placed under the sample to collect the dripping water droplets.

Simulation: The simulation results were completed by software COMSOL Multiphysics 5.5. In the setting of simulation software, 2D space latitude was selected, solid heat transfer module and solid mechanics module were selected for physical field, and thermal expansion module was added for multiple physical fields. The color legend in the simulation results indicated the magnitude of the stress, which was normalized.

Supporting Information

Supporting Information is available from the Wiley Online Library or from the author.

Conflict of Interest

The authors declare no conflict of interest.

Data Availability Statement

The data that support the findings of this study are available from the corresponding author upon reasonable request.

[1] a) D. G. Hwang, M. D. Bartlett, *Sci. Rep.* **2018**, *8*, 3378; b) N. An, A. G. Domel, J. Zhou, A. Rafsanjani, K. Bertoldi, *Adv. Funct. Mater.* **2019**, *30*, 1906711; c) Y. Tang, G. Lin, S. Yang, Y. K. Yi, R. D. Kamien, J. Yin, *Adv. Mater.* **2017**, *29*, 1604262; d) B. Florijn, C. Coulais, M. van Hecke, *Phys. Rev. Lett.* **2014**, *113*, 175503.

[2] a) R. Ma, C. Wu, Z. L. Wang, V. V. Tsukruk, *ACS Nano* **2018**, *12*, 9714; b) A. Rafsanjani, L. Jin, B. Deng, K. Bertoldi, *Proc. Natl. Acad. Sci. USA* **2019**, *116*, 8200; c) D.-G. Hwang, M. D. Bartlett, *Sci. Rep.* **2018**, *8*, 3378; d) T. Mullin, S. Deschanel, K. Bertoldi, M. C. Boyce, *Phys. Rev. Lett.* **2007**, *99*, 084301.

[3] a) Y. Zhang, Z. Yan, K. Nan, D. Xiao, Y. Liu, H. Luan, H. Fu, X. Wang, Q. Yang, J. Wang, *Proc. Natl. Acad. Sci. USA* **2015**, *112*, 11757; b) Y. Cho, J.-H. Shin, A. Costa, T. A. Kim, V. Kunin, J. Li, S. Y. Lee, S. Yang, H. N. Han, I.-S. Choi, *Proc. Natl. Acad. Sci. USA* **2014**, *111*, 17390; c) M. A. Dias, M. P. McCarron, D. Rayneau-Kirkhope, P. Z. Hanakata, D. K. Campbell, H. S. Park, D. P. Holmes, *Soft Matter* **2017**, *13*, 9087; d) L. Jin, A. E. Forte, B. Deng, A. Rafsanjani, K. Bertoldi, *Adv. Mater.* **2020**, *32*, 2001863; e) G. P. Choi, L. H. Dudte, L. Mahadevan, *Nat. Mater.* **2019**, *18*, 999.

[4] M. K. Blees, A. W. Barnard, P. A. Rose, S. P. Roberts, K. L. McGill, P. Y. Huang, A. R. Ruyack, J. W. Kevek, B. Kobrin, D. A. Muller, *Nature* **2015**, *524*, 204.

[5] Z. Liu, H. Du, J. Li, L. Lu, Z.-Y. Li, N. X. Fang, *Sci. Adv.* **2018**, *4*, eaat4436.

[6] A. Rafsanjani, K. Bertoldi, *Phys. Rev. Lett.* **2017**, *118*, 084301.

[7] X. Wang, X. Guo, J. Ye, N. Zheng, P. Kohli, D. Choi, Y. Zhang, Z. Xie, Q. Zhang, H. Luan, K. Nan, B. H. Kim, Y. Xu, X. Shan, W. Bai, R. Sun, Z. Wang, H. Jang, F. Zhang, Y. Ma, Z. Xu, X. Feng, T. Xie, Y. Huang, Y. Zhang, J. A. Rogers, *Adv. Mater.* **2019**, *31*, 1805615.

[8] a) L. Mizzi, K. M. Azzopardi, D. Attard, J. N. Grima, R. Gatt, *Physica Status Solidi RRL* **2015**, *9*, 425; b) S. Shan, S. H. Kang, Z. Zhao, L. Fang, K. Bertoldi, *Extreme Mech. Lett.* **2015**, *4*, 96.

[9] A. Lamoureux, K. Lee, M. Shlian, S. R. Forrest, M. Shtein, *Nat. Commun.* **2015**, *6*, 8092.

[10] K.-B. Kim, Y.-J. Lee, A. Costa, Y.-K. Lee, T.-S. Jang, M.-G. Lee, Y.-C. Joo, K. H. Oh, J. Song, I.-S. Choi, *Adv. Eng. Mater.* **2019**, *21*, 1900206.

[11] H. Zhao, K. Li, M. Han, F. Zhu, A. Vázquez-Guardado, P. Guo, Z. Xie, Y. Park, L. Chen, X. Wang, *Proc. Natl. Acad. Sci. USA* **2019**, *116*, 13239.

[12] a) K. Virk, A. Monti, T. Trehard, M. Marsh, K. Hazra, K. Boba, C. Remillat, F. Scarpa, I. Farrow, *Smart Mater. Struct.* **2013**, *22*, 084014; b) B. Gao, J. Chi, H. Liu, Z. Gu, *Sci. Rep.* **2017**, *7*, 7255; c) K. Xu, Y. Lu, S. Honda, T. Arie, S. Akita, K. Takei, *J. Mater. Chem. C* **2019**, *7*, 9609.

[13] a) N. An, A. G. Domel, J. Zhou, A. Rafsanjani, K. Bertoldi, *Adv. Funct. Mater.* **2020**, *30*, 1906711; b) P. Celli, C. McMahan, B. Ramirez, A. Bauhofer, C. Naify, D. Hofmann, B. Audoly, C. Daraio, *Soft Matter* **2018**, *14*, 9744.